Preparation and Performance of ZnO and ZnO/MnO₂ Nanostructures as Anode Electrodes in DSSCs

Suaad Abd Mahdi Abd Noor[1*] and Amer Muosa Juda Al-Shamari[2]

[1]*Pharmacology College, University of Kufa, Najaf 54001, Iraq*

[2]*Department of Chemistry, College of Science, University of Kufa, Najaf 54001, Iraq*

* Corresponding author:

tel: +964-7831130620
email: Suaad.toobi@uokufa.edu.iq

Abstract: *Nanoparticles and nanocomposites prepared by the hydrothermal method (ZnO, ZnO/MnO₂) were used to build dye-sensitized solar cells (DSSCs), which were used as photoelectrodes using two natural dyes as the absorbent media: red (*Hibiscus sabdariffa*) and green (*Apium graveolens*). The results showed the efficiency of the green dye in DSSCs is superior to the red dye in terms of conversion efficiency (η). The purpose of the study is to improve the performance of dye solar cells. The properties of nanomaterials were studied by X-ray diffraction (XRD), scanning electron microscopy (FE-SEM), and transmission electron microscopy (TEM) for the analysis of ZnO NPs and ZnO/MnO₂, whereas the sizes of the prepared materials are within the size of 1–100 nm. The solar cell parameters were obtained from simple (I-V) measurements for nanomaterials prepared using two-dye DSSCs where I_{sc} represents the short circuit current through the solar cell when the voltage across the solar cell is zero, and V_{oc} represents the open circuit voltage across the solar cell and is the maximum voltage available from the solar cell. The photoelectrochemical properties of the two dye DSSCs in this study were calculated at 22.53 mW/cm² of the light intensity.*

Keywords: *semiconductors; nano chemical synthesis; photoelectrodes; establishment of DSSCs; conversion efficiency*

■ INTRODUCTION

Concerns about greenhouse gas emissions and climate change have increased along with the corresponding energy demands as the world's population keeps growing [1-2]. Dye-sensitized solar cells (DSSCs) [3], organic solar cells (OSCs) [4], and perovskite solar cells (PSCs) [5-6] are examples of third-generation photovoltaic technologies that have been developed using inexpensive, simple, plentiful materials, and scalable fabrication techniques. Nonetheless, they are perfect for portable electronics [7] since they can be produced as small, light, and flexible solar modules [8-9]. Furthermore, they are potential for ambient energy harvesting for the wireless sensors used in internet of things (IoT) devices due to their excellent efficiency in low light, which beats other existing technologies under typical indoor conditions. [7,10-12]. In this article, new

materials that can be used to create high-performance DSSC-based photovoltaic devices have recently made strides [13-22]. Together with the increased possibilities for their potential incorporation in portable electronics, wireless sensor networks, and IoT devices [12], innovative DSSC device designs that have emerged in recent years using alternate redox shuttles and catalyst materials are discussed. The development in the related materials is also compiled in this study, showing how each functional component of a DSSC has been enhanced using new materials and production techniques. Also, a method for creating a novel cell design is given, which might be accomplished soon with the use of scalable fabrication techniques. Hydrothermal was used to create nanomaterials in this study because of the ease and speed of the method as well as the formation of high-purity nanomaterials in a short time.

■ EXPERIMENTAL SECTION

Materials

Chemicals used in the preparation of zinc oxide nanoparticles included $Zn(NO_3)_2 \cdot 6H_2O$ purchased from Thomas baker (India) with a purity of 98%, sodium hydroxide (NaOH) from Fluka with a purity of 97%, and ethanol (C_2H_5OH) Riedel-De-Haen AG, (Germany), 100% pure.

The ZnO/MnO_2 nanocomposite was prepared using manganese chloride tetrahydrate ($MnCl_2 \cdot 4H_2O$) from Thomas baker (India) with a purity of 98%, and the zinc chloride ($ZnCl_2$) from Thomas baker (India) with a purity of 99%. In addition, urea (CH_4N_2O) from Thomas baker (India) with a purity of 98%, and ethylene glycol ($C_2H_6O_2$) Merck, (Germany) with a purity of 99.9% were used as well. The materials used in the preparation and application of solar cells included iodine (I_2) from Merck, (Germany) with a purity of 97%, potassium iodide (KI) from Thomas baker (India) with a purity of 97%, and acetic acid (CDH-INDIA) with a purity of 97%.

Instrumentation

A device autoclave (China), centrifuge Hettich EBA20 (Made in Germany), and field emission scanning electron microscopy (FESEM) TESCAN MIRA3 Hv 300 Zeiss (Made in Germany) were used in this study. A magnetic-stirrer hot plate VS-130-SH(vision)/scientific co, LTD (Korea), programmable Keithley electrometer (2400)Tektronix Company, and pH-Meter HI 96107 Water-Tester Reverse Osmosis/Hanna-Instrumentals (China) were used in this work. A sensitive balance electronic balance type ABS 120-4 Kern & Sohn GmbH, transmission electron microscopy (TEM): Zeiss EM 10 C, 100 kV (Germany), and the electrical furnace (CARBOLITE) homemade were used in this study. A UV-vis spectrophotometer single beam EMCLAB-11-U.V-1100.Vis 200–1100 nm sinco (Made in Germany), UV-vis spectrophotometer double beam SCINCO Mega-2100 (Korea), volt-meter DT-9205A CE Auto Power, and X-ray diffraction (XRD) 2700 AB Haoyuan Co. (China) were used in this work.

Procedure

Synthesis ZnO of nanoparticles using the hydrothermal method

ZnO nanoparticles are synthesized using hydrothermal technology. The materials used are $Zn(NO_3)_2 \cdot 6H_2O$ and NaOH pellets. Throughout the experiment, all ingredients needed to make the ZnO nanoparticles were diluted in deionized water (DIW). Zinc nitrate solutions at a concentration of 0.5 M were prepared with continuous stirring for 30 min using a mild magnetic stirrer to completely dissolve $Zn(NO_3)_2 \cdot 6H_2O$ in 30 mL of DIW. While this was happening, 30 mL of DIW was used to prepare a 5 M NaOH solution by agitating it for the same amount of time that the $Zn(NO_3)_2$ granules were dispersed. The NaOH solution is gradually added to the $Zn(NO_3)_2$ solution with continuous stirring until the pH of the reactants reaches 12. This solution mixture is placed in a Teflon-lined autoclave made of stainless steel with a capacity of 70 mL and heated to 100 °C for 2 h in the electric oven. Then, we take out the autoclave and let it cool down gradually to room temperature. After washing the precipitate repeatedly with deionized water and ethanol, it was dried and collected [23-28].

Preparation of ZnO/MnO₂ nanocomposites by the hydrothermal method

A hydrothermal technique was used to produce the ZnO/MnO_2 nanocomposite. The materials, 2.968 g of $MnCl_2 \cdot 4H_2O$, 6.133 g of $ZnCl_2$, and 2.342 g of CH_4N_2O, were mixed and dissolved in 150 mL of $C_2H_6O_2$ under constant stirring for 30 min at 350 rpm under ambient conditions. Then the solution is transferred to an autoclave made of stainless steel and Teflon. The autoclave is closed and left in the oven for 24 h at a temperature of 200 °C. Then, the autoclave is taken out from the oven and left to cool at room temperature. Afterwards, the solution and the precipitate are separated by a centrifuge. Then, DIW mixed with ethanol is used to wash the sample several times until a precipitate is produced. The resulting material is then dried at 100 °C, crushed, and subjected to calcination at

600 °C for 6 h. After drying and cooling, the ZnO/MnO₂ nanocomposites appeared as a dark brownish-colored powder [29].

■ RESULTS AND DISCUSSION

Characterization of Prepared Compounds

XRD analysis

The density and full breadth at half the maximum size and position were found through analysis of the XRD results. Peaks at 2θ, 31.67°, 34.34°, 36.20°, 47.46°, 56.54°, 62.83°, and 67.91°, respectively, were observed in nine diffractions and corresponded to crystal levels of (100), (002), (101), (102), (110), (103), and (112). Broad neutrality and a sharper peak without any peak twisting were observed at (101) peaks. The analysis was that these many peaks showed crystals with irregular orientation. ZnO nanoparticles with an average crystal volume of D

were created using the Debye-Scherer formula [30]. Hexagonal nanostructures are observed in ZnO. The XRD results obtained for the ZnO nanoparticles are consistent with previous literary studies (Fig. 1) because of their strong and narrow diffraction peaks, particularly in (100), (002), and (003). The XRD data breakdown demonstrates that the ZnO nanoparticles sample has a high degree of crystalline quality (101). Fig. 2 illustrates how XRD was used to describe the crystalline nature and crystal phases of the ZnO/MnO₂. The diffraction peaks show that there are polycrystalline MnO₂ and ZnO crystal planes present. According to sources, the composite consists of a cubic type MnO₂ and a hexagonal phase of wurtzite type ZnO (JCPDS card number: 65-3411) and (JCPDS card number: 39-0375) [31] Using Scherrer's formula, the average crystal size ranges between 15.47 and 66.62 nm.
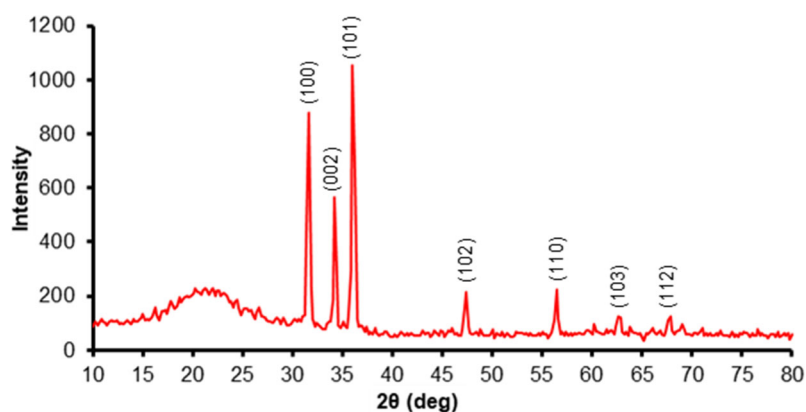
Fig 1. X-ray diffraction pattern of ZnO nanostructures
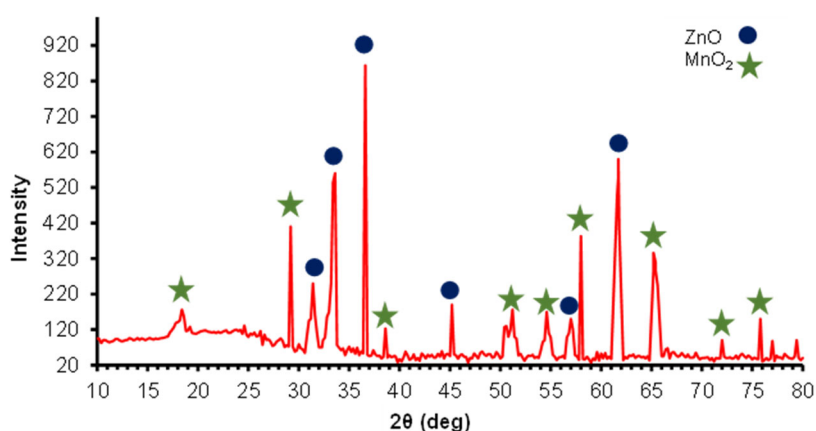
Fig 2. X-ray diffraction pattern of ZnO/MnO₂ nanocomposite

FE-SEM analysis

Fig. 3 displays FE-SEM images of ZnO nanostructures and ZnO/MnO$_2$ nanocomposites created. The typical diameter is 23.63 nm, more proof that ZnO is formed as a tangle of nanoparticles may be found in Fig. 3. The microstructural and textural properties of the prepared samples were decided by consulting the FESEM micrographs recorded at various scales. Fig. 4 shows the FESEM images of ZnO/MnO$_2$ at different magnification values, which demonstrated that the nanocomposite particles are composed of highly fibrous, gritty, and porous microstructures of 13–65 nm diameters with

vastly bumpy and uneven surfaces. Due to this, the surface area of the prepared is enhanced which has facilitated the adsorption and catalytic performance greatly.

TEM analysis

Analysis of TEM was employed to evaluate the created nanoparticles and nanocomposite materials. Fig. 5 illustrates the spherical shape of ZnO nanoparticles with sizes between 17.99 and 77.40 nm. The nanoparticles of the ZnO/MnO$_2$ nanocomposite are shown in Fig. (6) in terms of their shapes and sizes, and they range in size from 62.48–68.99 nm.
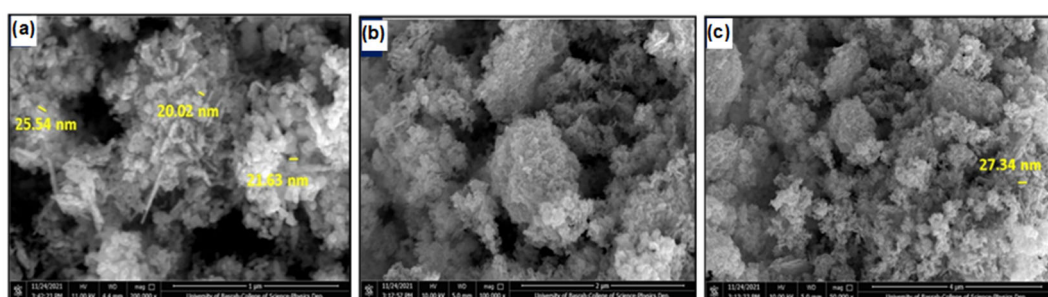
Fig 3. FE-SEM images of ZnO nanoparticles with a magnification of (a) 1 μm, (b) 2 μm, and (c) 4 μm
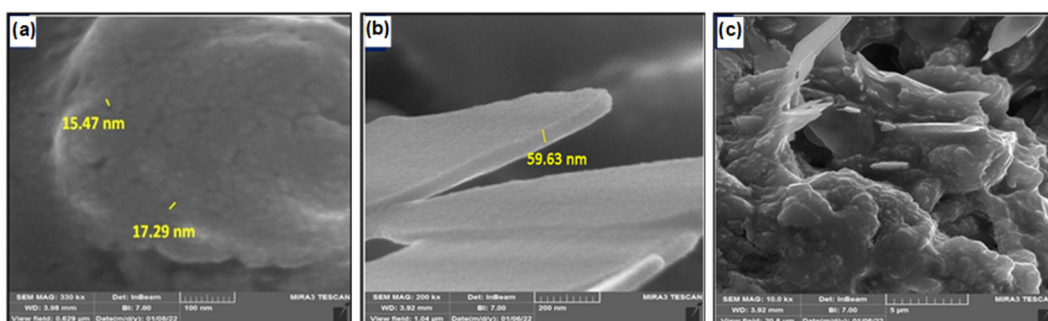
Fig 4. FE-SEM images of ZnO/MnO$_2$ nanocomposite with a magnification of (a) 100 nm, (b) 200 nm, and (c) 5 μm
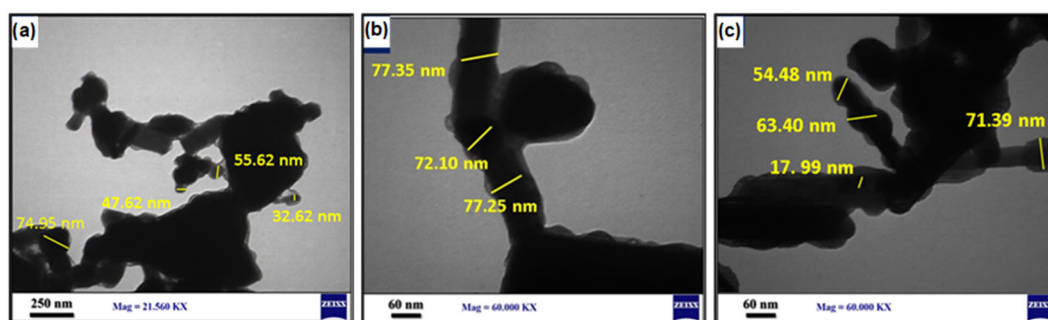
Fig 5. TEM images of ZnO nanoparticle with a magnification of (a) 250 nm, (b) 60 nm, and (c) 60 nm and an image of the oxide nanoparticles from another direction

Fabrication of Dye-Sensitized Solar Cells

In order to prepare DSSCs, ZnO nanoparticles and ZnO/MnO_2 nanocomposite were synthesized in the study and employed as a photoelectrode with two natural dyes as absorbent media: red dye from *Hibiscus sabdarriffa* and green dye from *Apium graveolens*. The I-V and characteristics of DSSCs made from nanosurfaces and natural dyes are shown in Fig. 7 and 8. As demonstrated in Table 1, the results indicated that the green dye improves the DSSCs conversion efficiency (η) over the red dye. There are various causes, one of which is the energy gap, which is different for the red and green dyes and is larger for the green dye. As a result, more ray wavelengths travel through the cells and are absorbed by the dye [32]. Second, since each of them has a unique surface area, there are differences between the surface areas of various nanomaterials. The effectiveness of the constructed DSSC rises as the green dye's adsorption on nanoscale surfaces increases. Moreover, due to the increased concentration of natural dye impurities, the current yield of DSSCs made with the natural red dye is lower than that of DSSCs rises as the green dye's adsorption on nanoscale surfaces increases. Moreover, due to the increased concentration of natural dye impurities, the
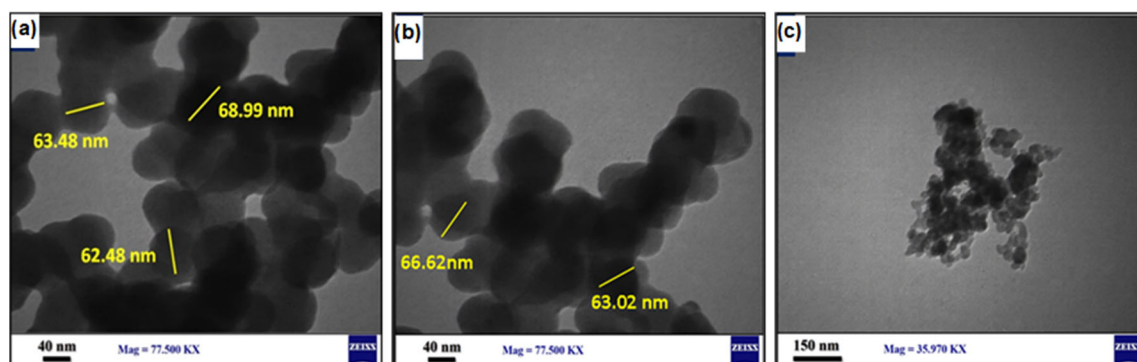
Fig 6. TEM images of ZnO/MnO_2 nanocomposite with a magnification (a) 40 nm, (b) 40 nm and an image of the oxide nanoparticles from another direction, and (c) 150 nm
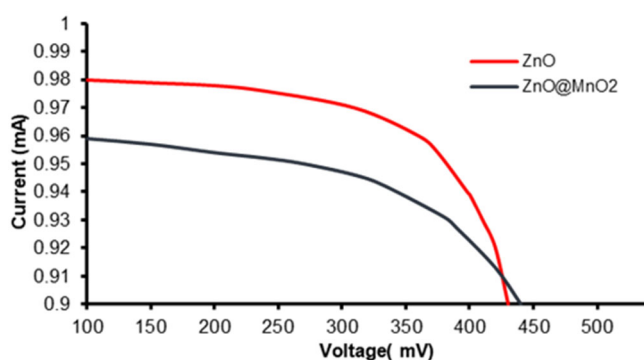
Fig 7. I-V characteristics of prepared DSSCs nanoparticles and nanocomposite prepared with red dye
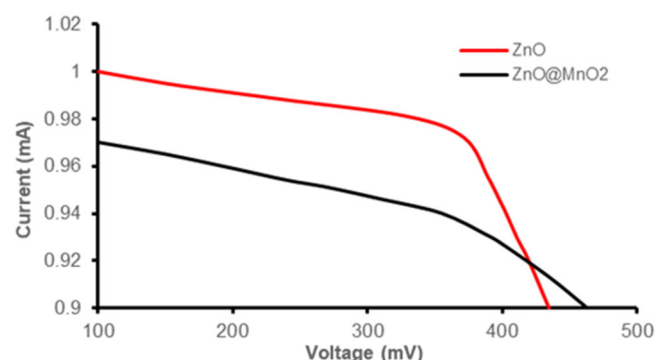
Fig 8. I-V characteristics of prepared DSSCs nanoparticles and nanocomposite prepared with green dye

Table 1. Photoelectrochemical characteristics of DSSCs (A = 5.4 cm² red dye and 4.5 cm² green dye) at 22.53 mW/cm² of light intensity

Catalyst/dye		I_{SC} (mA)	V_{oc} (V)	I_{max} (mA)	V_{max} (V)	P_{max}	FF	η %
ZnO	Red dye	0.980	430	0.974	368	358.43	0.8506	0.6640
	Green dye	1.000	435	0.980	380	372.40	0.8561	0.8276
ZnO/MnO_2	Red dye	0.959	440	0.946	360	340.56	0.8071	0.6310
	Green dye	0.970	463	0.938	365	342.37	0.7623	0.7610

current yield of DSSCs made with the natural red dye is lower than that of DSSCs made with the green dye [33]. Also, the low intensity of 22.53 mW/cm² of the light source used is another factor contributing to the low value found for the manufactured DSSCs and the use of carbon as the cathode electrode on the FTO solar cell's rear surface. Moreover, a conduction electrolyte composed of an I_2/iodide solution is created. DSSCs produced using Keithley 2400 were used to measure the photovoltaic performance (Fig. 9). Most solar cell parameters can be obtained from simple I-V measurements. Table 1 shows the IV measurement of solar cells under forward prejudice and brightness. The short circuit current (I_{sc}) is the current through the solar cell when the voltage across the solar cell is zero. The open circuit voltage (V_{oc}) is the voltage across the solar cell when the current through the solar cell is zero and it is the maximum voltage available from the solar cell [34]. The maximum power point (P_{max}) is the state under which the solar cell generates its maximum power. The current and voltage in this condition are defined as I_{max} and V_{max}, respectively. The fill factor (FF) and the conversion efficiency (η) are metrics used to characterize the performance of the solar cell [35]. The fill factor is defined as the ratio of P_{max} divided by the product of V_{oc} and I_{sc}. The conversion efficiency is defined as the ratio of P_{max} to the product of the input light irradiance (E) and the solar cell surface area (Ac) (see Eq. (1–4)) [36].

$$FF = \frac{P_{max}}{V_{oc} \times J_{sc}} \tag{1}$$

$$\eta = \frac{V_{oc} \times J_{sc} \times FF}{E} \tag{2}$$

$$FF = \frac{V_{max} \times J_{max}}{V_{oc} \times J_{sc}} \tag{3}$$

$$\%\eta = \frac{V_{oc} \times J_{sc} \times FF}{P_{in}} \tag{4}$$

Preparation of the Anode Electrodes

As mentioned earlier, the hydrothermal process is used to prepare the nanomaterials. A small amount of prepared nanomaterials is added and mixed with acetic acid and DIW (paste form) and spread on FTO glass plates as an anode electrode, one of the types of solar cells, leaving the cell edges not coated with the nanomaterial.

Fig 9. The measurement setup of the solar cells under the light effect using the Keithley device

Then, the solar cell is placed in an oven at a temperature of 40–50 °C to dry sufficiently. The anode electrode prepared from the nanosurface and the FTO glass was immersed in the red dye solution (the first dye) in the vessel to allow it to adhere to the surface of the nanomaterial for 24 h in a dark place. Then, the solar cells were removed from the dye solution the next day and also dried in a dark place to obtain the anode electrode. The prepared binary nanocomposite (ZnO/MnO_2) goes through the same steps to form the anode electrode in this way with the two dyes.

In order to prepare the cathode electrode, carbon (craft) is applied to the solar cell's surface, leaving the edges unaffected. The cathode pole was therefore furnished.

■ **CONCLUSION**

ZnO nanoparticles and ZnO/MnO_2 nanocomposites were developed using a single-step hydrothermal process. ZnO nanoparticles and ZnO/MnO_2 nanocomposites have been used as electrodynamic catalysts, and the effectiveness of nanomaterials (semiconductors) in the formation of DSSCs has been investigated. The use of solar cells in daily life applications was also performed because of their wide characteristics in terms of surface area and smallness, size and the power it provides. The study also shows the possibility of producing nanomaterials in several ways, including the simple chemical method. To know the effectiveness of the green dye on DSSCs compared to the red dye in terms of transduction efficiency (η). The effect of prepared ZnO nanoparticles and ZnO/MnO_2 nanocomposites on the conversion efficiency (η) with the red (*Hibiscus sabdariffa*) and

green (*Apium Gravolens*) dyes was studied. One of the benefits of using different characterizations is to know the nature of the surfaces of nanomaterials and their effectiveness as photoelectrodes, in addition to their crystal structures and different shapes. We also conclude the possibility of developing solar cells using various nanomaterials to improve their work and electrical properties and use them in the future to provide energy and electricity at the lowest cost. The functionality improvement in solar cells is also affected by the size of the nanocrystals during the solid-to-solid phase transition. Therefore, phase control is a critical step.

■ ACKNOWLEDGMENTS

■ AUTHOR CONTRIBUTIONS

The authors made equal contributions to conceptualization, design, data acquisition, data analysis and interpretation based on current and past scientific facts and studies, participated in the drafting of articles or critical review of important intellectual content, agreed to submit them to the current magazine; gave its final approval for the publication of the version, and agreed to be responsible for all aspects of the work. Dr. Amer Muosa Juda Al-Shamari researcher had the idea of researching, proposing the method of work and checking scientific information after the research had been completed. Researcher Suaad Abd Al-Mahdi conducted the proposed methods of research and collected the results, as well as provided financial contribution to the completion of the research.

■ REFERENCES

[1] Wu, Y., Li, C., Tian, Z., and Sun, J., 2020, Solar-driven integrated energy systems: State of the art and challenges, *J. Power Sources*, 478, 228762.

[2] Yan, N., Zhao, C., You, S., Zhang, Y., and Li, W., 2020, Recent progress of thin-film photovoltaics for indoor application, *Chin. Chem. Lett.*, 31 (3), 643–653.

[3] Metwally, R.A., El Nady, J., Ebrahim, S., El Sikaily, A., El-Sersy, N.A., Sabry, S.A., and Ghozlan, H.A., 2023, Biosynthesis, characterization and optimization of TiO_2 nanoparticles by novel marine halophilic *Halomonas* sp. RAM2: Application of natural dye-sensitized solar cells, *Microb. Cell Fact.*, 22 (1), 78.

[4] Liu, S., Yuan, J., Deng, W., Luo, M., Xie, Y., Liang, Q., Zou, Y., He, Z., Wu, H., and Cao, Y., 2020, High-efficiency organic solar cells with low non-radiative recombination loss and low energetic disorder, *Nat. Photonics*, 14 (5), 300–305.

[5] Wang, S.Y., Chen, C.P., Chung, C.L., Hsu, C.W., Hsu, H.L., Wu, T.H., Zhuang, J.Y., Chang, C.J., Chen, H.M., and Chang, Y.J., 2019, Defect passivation by amide-based hole-transporting interfacial layer enhanced perovskite grain growth for efficient *p-i-n* perovskite solar cells, *ACS Appl. Mater. Interfaces*, 11 (43), 40050–40061.

[6] Omer, M.I., Ye, T., Li, X., Ma, S., Wu, D., Wei, L., Tang, X., Ramakrishna, S., Zhu, Q., Xiong, S., Xu, J., Vijila, C., and Wang, X., 2023, Two quasi-interfacial *p-n* junctions observed by a dual-irradiation system in perovskite solar cells, *npj Flexible Electron.*, 7 (1), 23.

[7] Liao, Y., Tian, N., Wang, J., Yao, D., Zheng, G., Zhou, B., Yang, Y., and Long, F., 2022, Performance enhancement of evaporated $CsPbI_2Br$ perovskite solar cells with a CuSCN hole transport layer via a cesium bromide buffer layer, *ACS Appl. Energy Mater.*, 5 (8), 9542–9548.

[8] Mishu, M.K., Rokonuzzaman, M., Pasupuleti, J., Shakeri, M., Rahman, K.S., Hamid, F.A., Tiong, S.K., and Amin, N., 2020, Prospective efficient ambient energy harvesting sources for IoT-equipped sensor applications, *Electronics*, 9 (9), 1345.

[9] Bardwell, M., Wong, J., Zhang, S., and Musilek, P., 2018, Design considerations for IoT-based PV charge controllers, *2018 IEEE World Congress on Services (SERVICES)*, San Francisco, CA, USA, 2-7 July 2018, 59–60.

Indones. J. Chem., 2023, 23 (6), 1618 - 1626

1625

[10] Michaels, H., Rinderle, M., Freitag, R., Benesperi, I., Edvinsson, T., Socher, R., Gagliardi, A., and Freitag, M., 2020, Dye-sensitized solar cells under ambient light powering machine learning: Towards autonomous smart sensors for the internet of things, *Chem. Sci.*, 11 (11), 2895–2906.

[11] Dhingra, S., Madda, R.B., Patan, R., Jiao, P., Barri, K., and Alavi, A.H., 2020, Internet of things-based fog and cloud computing technology for smart traffic monitoring, *Internet Things*, 14, 100175.

[12] Lee, H.K.H., Barbé, J., Meroni, S.M.P., Du, T., Lin, C.T., Pockett, A., Troughton, J., Jain, S.M., De Rossi, F., Baker, J., Carnie, M.J., McLachlan, M.A., Watson, T.M., Durrant, J.R., and Tsoi, W.C., 2019, Outstanding indoor performance of perovskite photovoltaic cells – Effect of device architectures and interlayers, *Sol. RRL*, 3 (1), 1800207.

[13] Prajapat, K., Dhonde, M., Sahu, K., Bhojane, P., Murty, V.V.S., and Shirage, P.M., 2023, The evolution of organic materials for efficient dye-sensitized solar cells, *J. Photochem. Photobiol., C*, 55, 100586.

[14] Meador, W.E., Liyanage, N.P., Watson, J., Groenhout, K., and Delcamp, J.H., 2023, Panchromatic NIR-absorbing sensitizers with a thienopyrazine auxiliary acceptor for dye-sensitized solar cells, *ACS Appl. Energy Mater.*, 6 (10), 5416–5428.

[15] Perrella, F., Li, X., Petrone, A., and Rega, N., 2023, Nature of the ultrafast interligands electron transfers in dye-sensitized solar cells, *JACS Au*, 3 (1), 70–79.

[16] Kumar, D., Parmar, K.P.S., and Kuchhal, P., 2020, Optimizing photovoltaic efficiency of a dye-sensitized solar cell (DSSC) by a combined (modelling-simulation and experimental) study, *Int. J. Renewable Energy Res.*, 10 (1), 165–174.

[17] Supriyanto, E., Kartikasari, H.A., Alviati, N., and Wiranto, G., 2019, Simulation of dye-sensitized solar cells (DSSC) performance for various local natural dye photosensitizers, *IOP Conf. Ser.: Mater. Sci. Eng.*, 515, 012048.

[18] Bashir, M.B.A., Rajpar, A.H., Salih, E.Y., and Ahmed, E.M., 2023, Preparation and photovoltaic evaluation of CuO@Zn(Al)O-mixed metal oxides for dye-sensitized solar cell, *Nanomaterials*, 13 (5), 802.

[19] Alizadeh, A., Roudgar-Amoli, M., Bonyad-Shekalgourabi S.M., Shariatinia, Z., Mahmoudi, M., and Saadat, F., 2022, Dye-sensitized solar cells go beyond using perovskite and spinel inorganic materials: A review, *Renewable Sustainable Energy Rev.*, 157, 112047.

[20] Lu, J., Liu, S., and Wang, M., 2018, Push-pull zinc porphyrins as light-harvesters for efficient dye-sensitized solar cells, *Front. Chem.*, 6, 00541.

[21] Kakiage, K., Aoyama, Y., Yano, T., Oya, K., Fujisawa, J., and Hanaya, M., 2015, Highly-efficient dye-sensitized solar cells with collaborative sensitization by silyl-anchor and carboxy-anchor dyes, *Chem. Commun.*, 51 (88), 15894–15897.

[22] Cao, Y., Liu, Y., Zakeeruddin, S.M., Hagfeldt, A., and Grätzel, M., 2018, Direct contact of selective charge extraction layers enables high-efficiency molecular photovoltaics, *Joule*, 2, 1108–1117.

[23] Abu Nayem, S.M., Shah, S.S., Chaity, S.B., Biswas, B.K., Nahar, B., Aziz, M.A., and Hossain, M.Z., 2022, Jute stick extract assisted hydrothermal synthesis of zinc oxide nanoflakes and their enhanced photocatalytic and antibacterial efficacy, *Arabian J. Chem.*, 15 (11), 104265.

[24] Zhou, Y., Xu, L., Wu, Z., Li, P., and He, J., 2017, Optical and photocatalytic properties of nanocrystalline ZnO powders synthesized by a low-temperature hydrothermal method, *Optik*, 130, 673–680.

[25] Raji, R., and Gopchandran, K.G., 2017, ZnO nanostructures with tunable visible luminescence: Effects of kinetics of chemical reduction and annealing, *J. Sci.: Adv. Mater. Devices*, 2 (1), 51–58.

[26] Selim, H., Nada, A.A., El-Sayed, M., Hegazey, R.M., Souaya, E.R., and Kotkata, M.F., 2018, The effect of ZnO and its nanocomposite on the performance of dye sensitized solar cell, *Nano Sci. Nano Technol.*, 12 (1), 122.

[27] Shanavas Khan, J., Asha Radhakrishnan, A., and Beena, B., 2018, Polyaniline/zinc oxide nanocomposite as a remarkable antimicrobial agent in contrast with PANI and ZnO, *Indian J. Adv. Chem. Sci.*, 6 (2), 71–76.

[28] Quadri, T.W., Olasunkanmi, L.O., Fayemi, O.E., Solomon, M.M., and Ebenso, E.E., 2017, Zinc oxide nanocomposites of selected polymers: Synthesis, characterization, and corrosion inhibition studies on mild steel in HCl solution, *ACS Omega*, 2 (11), 8421–8437.

[29] Anantha, M.S., Kiran Kumar, S.R., Anarghya, D., Venkatesh, K., Santosh, M.S., Yogesh Kumar, K., and Muralidhara, H.B., 2021, ZnO@MnO$_2$ nanocomposite modified carbon paste electrode for electrochemical detection of dopamine, *Sens. Int.*, 2, 100087.

[30] Bulcha, B., Leta Tesfaye, J., Anatol, D., Shanmugam, R., Dwarampudi, L.P., Nagaprasad, N., Bhargavi, V.L.N., and Krishnaraj, R., 2021, Synthesis of zinc oxide nanoparticles by hydrothermal methods and spectroscopic investigation of ultraviolet radiation protective properties, *J. Nanomater.*, 2021, 8617290.

[31] Acharyya, S., Dey, S., Nag, S., and Guha, P.K., 2018, ZnO cladded MnO$_2$ based resistive sensor device for Formaldehyde sensing, *2018 IEEE SENSORS*, New Delhi, India, 28-31 October 2018, 1–4.

[32] Lokman, M.Q., Shafie, S., Shaban, S., Ahmad, F., Jaafar, H., Mohd Rosnan, R., Yahaya, H., and Abdullah, S.S., 2019, Enhancing photocurrent performance based on photoanode thickness and surface plasmon resonance using Ag-TiO$_2$ nanocomposites in dye-sensitized solar cells, *Materials*, 12 (13), 2111.

[33] Schöttner, L., Nefedov, A., Yang, C., Heissler, S., Wang, Y., and Wöll, C., 2019, Structural evolution of α-Fe$_2$O$_3$ (0001) surfaces under reduction conditions monitored by infrared spectroscopy preview on related iron oxide, *Front. Chem.*, 7, 00451.

[34] Fang, Y., Ma, P., Cheng, H., Tan, G., Wu, J., Zheng, J., Zhou, X., Fang, S., Dai, Y., and Lin, Y., 2019, Synthesis of low-viscosity ionic liquids for application in dye-sensitized solar cells, *Chem. - Asian J.*, 14 (23), 4201–4206.

[35] Rangel, D., Gallegos, J.C., Vargas, S., García, F., and Rodríguez, R., 2019, Optimized dye-sensitized solar cells: A comparative study with different dyes, mordants and construction parameters, *Results Phys.*, 12, 2026–2037.

[36] Abdul-Sajad Al-Hachamy, F.A., 2020, Preparation of High Activity Binary and Ternary MgO Nanocomposites Catalysts and Their Environmental Application, *Dissertation*, College of Science, University of Kufa.